OPEN

Cell Death and Differentiation (2015) 22, 351–363

www.nature.com/cdd

Depletion of white adipocyte progenitors induces beige adipocyte differentiation and suppresses obesity development

AC Daquinag[1], C Tseng[1], A Salameh[1], Y Zhang[1], F Amaya-Manzanares[1], A Dadbin[1], F Florez[1], Y Xu[1], Q Tong[1] and MG Kolonin*,[1]

Overgrowth of white adipose tissue (WAT) in obesity occurs as a result of adipocyte hypertrophy and hyperplasia. Expansion and renewal of adipocytes relies on proliferation and differentiation of white adipocyte progenitors (WAP); however, the requirement of WAP for obesity development has not been proven. Here, we investigate whether depletion of WAP can be used to prevent WAT expansion. We test this approach by using a hunter-killer peptide designed to induce apoptosis selectively in WAP. We show that targeted WAP cytoablation results in a long-term WAT growth suppression despite increased caloric intake in a mouse diet-induced obesity model. Our data indicate that WAP depletion results in a compensatory population of adipose tissue with beige adipocytes. Consistent with reported thermogenic capacity of beige adipose tissue, WAP-depleted mice display increased energy expenditure. We conclude that targeting of white adipocyte progenitors could be developed as a strategy to sustained modulation of WAT metabolic activity.
Cell Death and Differentiation (2015) **22,** 351–363; doi:10.1038/cdd.2014.148; published online 24 October 2014

Obesity, a medical condition predisposing to diabetes, cardiovascular diseases, cancer, and complicating other life-threatening diseases, is becoming an increasingly important social problem.[1–3] Development of pharmacological approaches to reduction of body fat has remained a daunting task.[4] Approved obesity treatments typically produce only moderate and temporary effects.[2,5] White adipocytes are the differentiated cells of white adipose tissue (WAT) that store triglycerides in lipid droplets.[6,7] In contrast, adipocytes of brown adipose tissue (BAT) dissipate excess energy through adaptive thermogenesis. Under certain conditions, white adipocytes can become partially replaced with brown-like 'beige' ('brite') adipocytes that simulate the thermogenic function of BAT adipocytes.[7,8] Obesity develops in the context of positive energy balance as a result of hypertrophy and hyperplasia of white adipocytes.[9]

Expansion and renewal of the white adipocyte pool in WAT continues in adulthood.[10,11] This process is believed to rely on proliferation and self-renewal of mesenchymal precursor cells[12] that we term white adipocyte progenitors (WAPs). WAPs reside within the population of adipose stromal cells (ASCs)[13] and are functionally similar to bone marrow mesenchymal stem cells (MSCs).[14–16] ASCs can be isolated from the stromal/vascular fraction (SVF) of WAT based on negativity for hematopoietic (CD45) and endothelial (CD31) markers.[17,18] ASCs support vascularization as mural/adventitial cells secreting angiogenic factors[5,19] and, unlike bone marrow MSCs, express CD34.[19,20] WAPs have been identified within the ASC population based on expression of mesenchymal markers, such as platelet-derived growth factor receptor-β (PDGFRβ, aka CD140b) and pericyte markers.[17,18] Recently, a distinct ASC progenitor population capable of differentiating into both white and brown adipocytes has been identified in WAT based on PDGFRα (CD140a) expression and lack of PDGFRβ expression.[21,22] The physiological relevance of the two precursor populations residing in WAT has not been explored.

We have previously established an approach to isolate peptide ligands binding to receptors selectively expressed on the surface of cell populations of interest.[23–27] Such cell-targeted peptides can be used for targeted delivery of experimental therapeutic agents *in vivo*. A number of 'hunter-killer' peptides[28] composed of a cell-homing domain binding to a surface marker and of $KLAKLAK_2$ (sequence KLAKLAKKLAKLAK), a moiety inducing apoptosis upon receptor-mediated internalization, has been described by our group.[26,29] Such bimodal peptides have been used for depletion of malignant cells and organ-specific endothelial cells in preclinical animal models.[26,30,31] Recently, we isolated a cyclic peptide WAT7 (amino acid sequence CSWKYWFGEC) based on its specific binding to ASCs.[20] We identified Δ-decorin (ΔDCN), a proteolytic cleavage fragment of decorin, as the WAT7 receptor specifically expressed on the surface of CD34+PDGFRβ+CD31-CD45- WAPs and absent on MSCs in other organs.[20]

Here, we investigated whether WAPs are required for obesity development in adulthood. By designing a new

[1]Center for Metabolic and Degenerative Diseases, The Brown Foundation Institute of Molecular Medicine, University of Texas Health Science Center at Houston, Houston, TX, USA

*Corresponding author: MG Kolonin, Center for Metabolic and Degenerative Diseases, The Brown Foundation Institute of Molecular Medicine, University of Texas Health Science Center at Houston, 1825 Pressler Street, Houston, TX 77030, USA. Tel: +1 713-500-3146; Fax +1 713-500-2424; E-mail: Mikhail.G.Kolonin@uth.tmc.edu

Abbreviations: BAT, brown adipose tissue; WAT, white adipose tissue; WAP, white adipocyte progenitor; MSC, mesenchymal stem cell; ASC, adipose stromal cell; SVF, stromal/vascular fraction; PDGFR, platelet-derived growth factor receptor; $KLAKLAK_2$, KLAKLAKKLAKLAK; DCN, decorin; i.p., intraperitoneal; s.c., subcutaneous; CLAMS, Comprehensive Lab Animal Monitoring System; DIO, diet-induced obesity; UCP1, uncoupling protein 1; Plin1, perilipin-1; shRNA, short hairpin RNA; TZD, thiazolidazines

Received 04.3.14; revised 29.7.14; accepted 06.8.14; Edited by M Piacentini; published online 24.10.14

hunter-killer peptide that directs $KLAKLAK_2$ to WAPs through WAT7/ΔDCN interaction, we depleted WAP in the mouse diet-induced obesity model. We demonstrate that WAP depletion suppresses WAT growth. We show that, in response to WAP deficiency, WAT becomes populated with beige adipocytes. Consistent with the reported thermogenic function of beige adipocytes,[32,33] the observed WAT remodeling is associated with increased energy expenditure. We identify a population of PDGFR*α*-positive, PDGFR*β*-negative ASCs reported recently[22] as a population surviving WAP depletion and responsible for WAT browning.

Results

Peptide D-WAT targets WAP in cell culture and *in vivo*. Incubation of adherent mouse ASCs with fluorophore-labeled WAT7 resulted in its intracellular accumulation (Figure 1a), suggesting that WAT7 coupled with a pro-apoptotic moiety could be used to deplete adipose progenitors. Based on the published approach,[26,30] a bimodal peptide $_d$WAT7-$KLAKLAK_2$ (termed D-WAT), composed of WAT7 and of $KLAKLAK_2$ domains linked via aminohexanoic acid, was synthesized with all amino acids as D-enantiomers to prevent proteolytic degradation. We used flow cytometric measurement of Apo-Trace uptake to show that D-WAT induces apoptosis of SVF isolated from mouse intraperitoneal (i.p.) WAT (Figure 1b). Similarly, a dose-dependent cytotoxicity of the peptide toward SVF from subcutaneous (s.c.) WAT was revealed (Figure 1c). Importantly, endothelial and hematopoietic cells of WAT, which can be distinguished from ASCs based on CD31 and CD45 expression, as well as morphology,[20,34] remained viable at D-WAT concentration lethal for ASC (Figure 1c). Upon treatment of mouse i.p. or s.c. WAT-derived cells adherent in culture, D-WAT killed ASCs within 12 h, whereas neither the homing domain WAT7 nor $KLAKLAK_2$ alone or a previously reported peptide CKGGRAKDC-$KLAKLAK_2$ (which does not target WAP)[26] induced ASC death (Figure 1d). Importantly, D-WAT did not induce death of cells derived from interscapular BAT (Figure 1d). These data indicate specificity of D-WAT for ASCs.

Next, we tested whether D-WAT can be used for targeting WAPs *in vivo* by administering peptide into mice and comparing their tissues with tissues from sham-treated animals. Flow cytometry revealed D-WAT-induced apoptosis in both s.c. and i.p. WAT, but not in interscapular BAT (Figure 1e). Whereas apoptosis was peptide dose dependent in WAT, background Apo-Trace signal was not dose dependent in control organs (Figure 1f). Leukocyte (CD45+) frequency in i.p. WAT was at least twice as high than in s.c. WAT in mice analyzed (Figure 1g), explaining why Apo-Trace+ cell frequency was lower in i.p. WAT. Increased sensitivity of s.c. ASCs to D-WAT could also partly result from D-WAT administration into the s.c. depot where it is likely to be transiently present at a higher concentration before distributing systemically. Apoptosis targeting to WAP was confirmed by immunofluorescence analysis of tissues with antibody against cleaved (Asp175) caspase 3. We detected apoptosis in perivascular cells of WAT surrounding the CD31-positive endothelial lumen, whereas only rare apoptotic cells were detected in liver and kidneys (Figure 1h). Using antibodies against DCN, we confirmed that the peptide treatment resulted in a depletion of perivascular ASCs while sparing the CD31-positive endothelium (Figure 1i). Combined, these data indicate that D-WAT induces apoptosis specifically in WAP.

WAP depletion inhibits WAT expansion. To test whether WAP depletion can suppress WAT expansion, we inspected the effect of D-WAT on diet-induced obesity (DIO) induction in C57BL/6 male mice that were fed high-fat diet throughout the 12-week experiment period. Mice were metronomically s.c. injected with D-WAT for 4 weeks; control animals were injected with saline. Peptide-treated and control groups displayed no difference in the total body mass at the end of the treatment (week 4). However, analysis of body composition by Echo MRI demonstrated a difference in fat mass between the groups (Figure 2a). Echo MRI measurements on animals monitored after treatment discontinuation demonstrated that accumulation of fat mass, but not of lean mass, was suppressed long term (week 12) in peptide-treated mice. Necropsy revealed comparatively smaller sizes and weights of i.p. and s.c. WAT pads in treated mice (Figure 2b), indicating that D-WAT treatment suppresses DIO development.

To confirm that WAP depletion underlies WAT growth suppression, we analyzed adherent SVF cells at week 8. The majority of viable SVF recovered from s.c. or i.p. WAT of treated mice had endothelial or monocyte morphology, whereas cells with ASC morphology were rare (Figure 2c). In contrast, recovery of cells with mesenchymal morphology from interscapular BAT and lungs was unaffected (Figure 2c).

Figure 1 D-WAT peptide induces ASC apoptosis. (**a**) Adherent ASCs from i.p. WAT were incubated with Cy3-labeled peptide WAT7 (red), washed, and subjected to anti-CD44 confocal immunofluorescence visualizing cell surface (green). Intracellular peptide (arrow) is indicated in *Z*-stack projections of median series. (**b**) Flow cytometric quantification of Apo-Trace uptake demonstrates i.p. SVF apoptosis induced by 0.05 mM D-WAT treatment; Control: untreated cells. (**c**) Phase contrast micrographs of s.c. SVF after 0.05 mM D-WAT treatment shows dead (Trypan blue positive) ASCs among viable monocytes (arrowheads) and endothelial cells (*). Plot on the right shows D-WAT dose dependence measured based on Trypan blue+ cell frequency. (**d**) Micrographs of indicated cells demonstrate apoptosis induced by D-WAT but not by the uncoupled $_d$WAT7 and $_d$$KLAKLAK_2$ domains or by Adipotide (CKGGRAKDC-$_d$$KLAKLAK_2$). Note D-WAT sensitivity of s.c. and i.p. ASCs but not of BAT-derived stroma. (**e** and **f**) Mice were s.c. injected with D-WAT or PBS (Control), and 48 h later tissues were analyzed. (**e**) Upon subsequent i.v. Apo-Trace injection, *in vivo* apoptosis was detected through flow cytometric analysis of identical cell numbers for control and treated tissues demonstrates D-WAT-induced apoptosis in s.c. and i.p. WAT, but not in BAT. (**f**) D-WAT dose-dependent apoptosis frequency observed for cells from s.c. and i.p. WAT, but not for control organs. (**g**) Flow cytometric analysis of matched numbers of s.c. and i.p. SVF from mice injected with D-WAT in (**e**) with PE-conjugated CD31 antibody and APC-Cy7-conjugated CD45 antibody demonstrates a higher frequency of leukocytes (CD45+CD31−) in i.p. WAT. (**h**) Immunofluorescence on sections of indicated tissues from D-WAT-treated mice with antibody against cleaved Caspase 3 (green) demonstrates apoptosis (arrows) in s.c. WAT perivascular cells. (**i**) The s.c. WAT section immunofluorescence with anti-decorin antibody (green) demonstrates loss of perivascular DCN-expressing cells (arrows) specifically in treated mice. Endothelium is stained with anti-CD31 antibody (red). Blue: nuclei. Scale bar: 50 μm

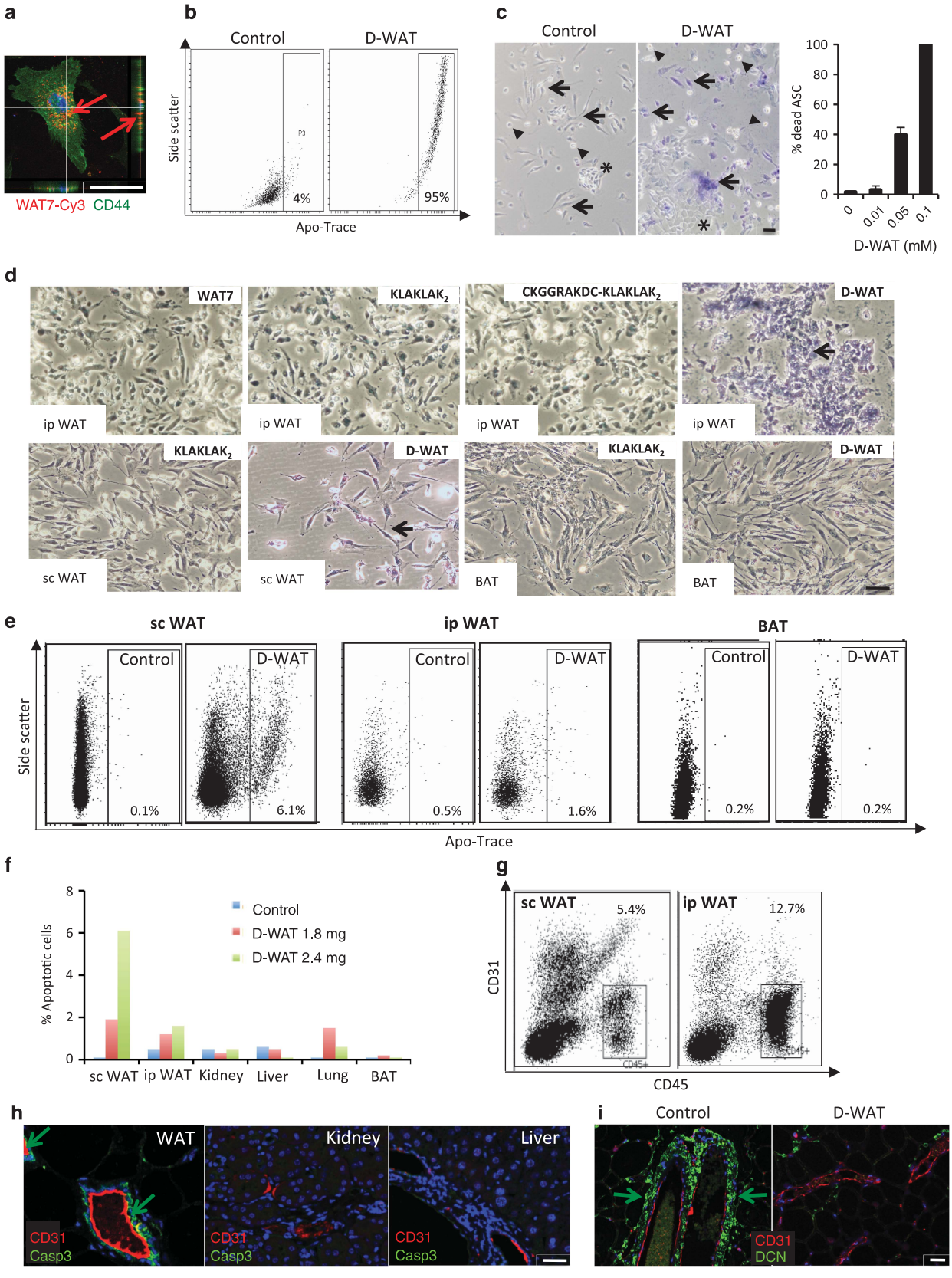
a
WAT7-Cy3 CD44
b
Control
D-WAT
Side scatter
P3
4%
95%
Apo-Trace
c
Control
D-WAT
% dead ASC
100
80
60
40
20
0
0
0.01
0.05
0.1
D-WAT (mM)
d
WAT7
KLAKLAK2
CKGGRAKDC-KLAKLAK2
D-WAT
ip WAT
sc WAT
BAT
e
sc WAT
ip WAT
BAT
Control
D-WAT
Side scatter
0.1%
6.1%
0.5%
1.6%
0.2%
0.2%
Apo-Trace
f
% Apoptotic cells
Control
D-WAT 1.8 mg
D-WAT 2.4 mg
sc WAT
ip WAT
Kidney
Liver
Lung
BAT
g
sc WAT
5.4%
ip WAT
12.7%
CD31
CD45
h
WAT
Kidney
Liver
CD31
Casp3
i
Control
D-WAT
CD31
DCN

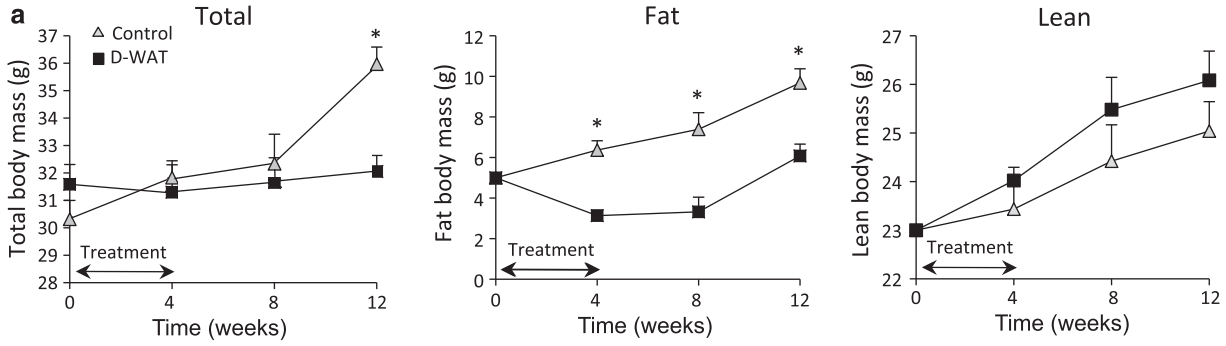
a
Total
Control
D-WAT
Total body mass (g)
Treatment
Time (weeks)
Fat
Fat body mass (g)
Lean
Lean body mass (g)

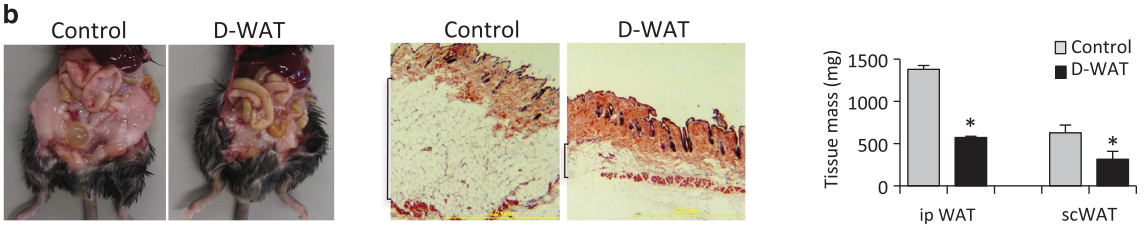
b
Control
D-WAT
Tissue mass (mg)
ip WAT
scWAT

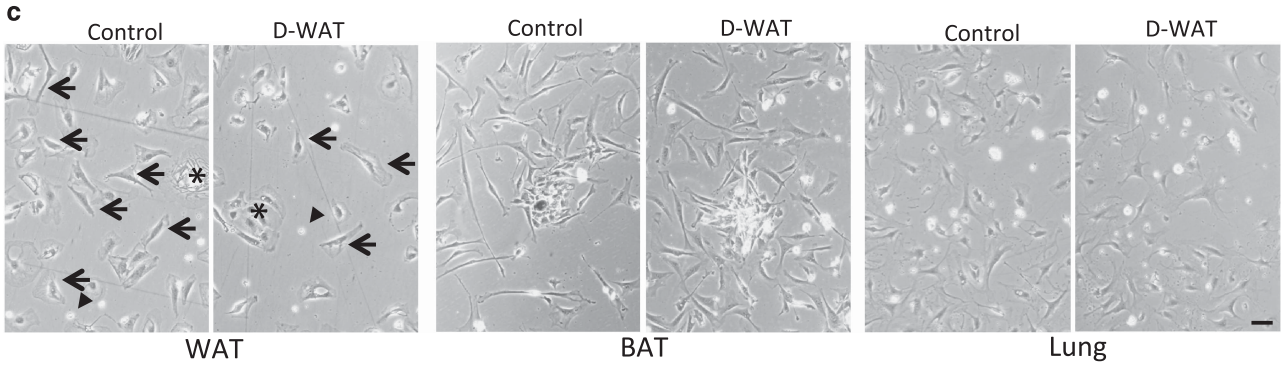
c
WAT
BAT
Lung

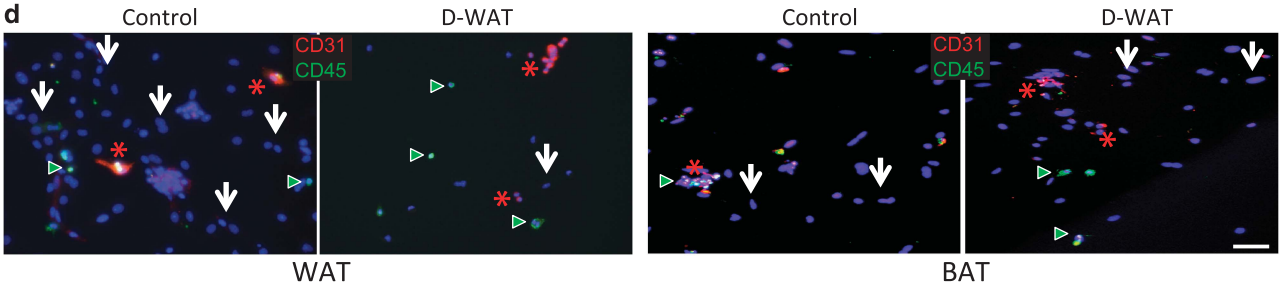
d
CD31
CD45
WAT
BAT

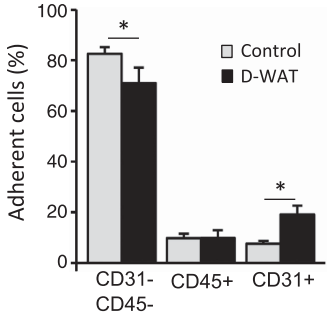
e
Adherent cells (%)
CD31-
CD45-
CD45+
CD31+

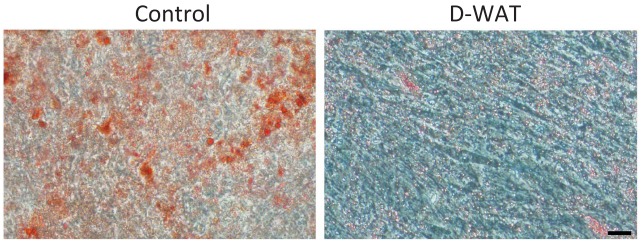
f
Control
D-WAT

We confirmed the selectivity of D-WAT *in vivo* by determining the frequency of ASCs among SVF cells remaining after peptide treatment (Figure 2d). Quantification showed that the ASC frequency was significantly reduced, whereas no decrease in the frequencies of endothelial cells (CD31+) or leukocytes (CD45+) was observed (Figure 2e). In contrast, D-WAT did not affect the CD31− CD45− stromal cells in interscapular BAT (Figure 2d). Upon subjecting the adherent SVF to white adipogenesis induction and subsequent Oil Red O staining, we observed a reduced frequency of adipocytes accumulating large lipid droplets in treated animals (Figure 2f). We have previously tested analogous hunter-killer peptides based on $KLAKLAK_2$ designed to target different cell populations.[26,29] As we have reported, neither uncoupled $_dKLAKLAK_2$ peptide nor $_dKLAKLAK_2$ domain fused with untargeted cyclic peptides have an effect on WAT or on DIO induction.[26] This indicates that $KLAKLAK_2$ targeting to WAP with WAT7 is required for the effect of D-WAT. Our data indicate that mice treated with D-WAT display deficient WAT growth due to WAP depletion.

WAP depletion prevents dyslipidemia but leads to hyperglycemia. Because WAT mass is a major factor in the regulation of lipid and sugar homeostasis, we analyzed a number of biochemical plasma variables in mice immediately after treatment discontinuation and at week 12. No significant differences in the basal levels of free fatty acids (FFA), glycerol, triglycerides (TG), and cholesterol were detected between control and peptide-treated animals (Figure 3a). Elevation in the steady-state plasma levels of insulin and glucose was detected in nonstarved animals (Figure 3a). However, no difference in fasting glucose tolerance was revealed between treated and control mice at both early and late time points (Figure 3b). We did not detect lipid intolerance upon intralipid infusion into fasted mice (Figure 3c). Increased systemic circulation of β-hydroxybutyrate was detected in treated mice (Figure 3d). This suggests that hyperlipidemia and ectopic fatty acid deposition is at least partly circumvented by their oxidation into ketone bodies. Stimulation of fatty acid utilization by D-WAT was also evident from steatosis apparent in the livers of control DIO but not in treated mice (Figure 3e). Triglyceride content was comparable in skeletal muscle of treated and control mice (Figure 3f). Analysis of feces revealed elevated triglyceride levels in stool of treated mice (Figure 3f). This indicates that both reduced fatty acid absorption and their increased breakdown contribute to prevention of dyslipidemia upon WAP depletion.

WAP depletion activates energy expenditure. As previously observed for other WAT mass reduction models,[35] the circulating level of leptin, secreted by white adipocytes, was significantly reduced in mice treated with D-WAT (Figure 4a). Consistent with the appetite-suppressing leptin function,[36,37] we observed increased food consumption for peptide-treated animals (Figure 4b). To test whether increased energy expenditure compensates for increased calorie intake in mice treated with D-WAT, we analyzed mice using a Comprehensive Lab Animal Monitoring System (CLAMS). Both oxygen consumption and carbon dioxide production were elevated upon treatment, and indirect calorimetry revealed a progressive increase in heat expenditure by treated mice (Figure 4c). Compared with control mice, higher heat generation was detected for peptide-treated mice during both dark and light cycles (Figure 4d). Consistent with increased thermogenesis, sensors implanted onto upper flanks of mice demonstrated higher daytime core body temperature (Figure 4e). Spontaneous locomotor activity was also elevated post treatment (Figure 4f).

WAP depletion results in WAT population with beige adipocytes. The level of locomotor activity increase (Figure 4f) is unlikely to explain the marked effects of D-WAT treatment on energy expenditure. Thus, we analyzed BAT to determine whether it is hypertrophic, which would account for increased thermogenesis. However, the size of interscapular BAT depots was not increased by treatment. As shown in Figure 5a, interscapular BAT in D-WAT-treated animals was visually less white, indicating lower lipid content. Indeed, BAT section analysis confirmed that lipid accumulation observed in control DIO mice was lower in D-WAT-treated animals (Figure 5b). Such 'browning' of BAT has been previously linked with improvement of its thermogenic function.[38] To address whether this is the case in WAP-depleted animals, we analyzed expression of uncoupling protein 1 (UCP1), a protein responsible for thermogenesis.[32] We could not detect a difference in expression frequency or intensity of UCP1, highly expressed in BAT adipocytes, between control and treated mice (Figure 5b).

A number of recent reports demonstrate that WAT 'browning' can lead to its metabolic activation.[38–42] It has been demonstrated that upon sympathetic nervous system stimulation, white adipocytes can become replaced with beige (brite) adipocytes that simulate brown adipocytes expending energy via adaptive thermogenesis.[8,32,33,43] We, therefore, considered a possibility that in our study increased thermogenesis in treated animals results from changes in WAT itself. Histological analysis revealed a trend for smaller adipocyte size in both s.c. and i.p. WAT of animals treated with D-WAT (Figure 5c).

Figure 2 WAP depletion suppresses WAT growth in DIO mice. Mice (15/group) maintained on high-fat diet underwent a 4-week treatment: twelve 200 μl s.c. injections (3/week) of 1 mM D-WAT (■) or PBS (control; □). (**a**) Changes in total, fat, and lean body mass during and after treatment. (**b**) Exposed i.p. WAT and intradermal s.c. WAT (bracketed in H&E-stained sections) hypotrophic in treated mice at week 8. WAT pad weights are quantified in the graph on the right. (**c**) Phase contrast micrographs of adherent cells recovered (week 8) from matched amount of i.p. WAT, interscapular BAT, and lung tissue showing reduced plating efficiency for WAT, but not for BAT or lung, of treated mice. Arrows indicate SVF cells with ASC morphology, arrowheads indicate monocytes, and asterisks indicate endothelial colonies. (**d**) Identification of mesenchymal stroma as CD31−CD45− cells with large nuclei (arrows) *versus* leukocytes as CD45+ cells (arrowheads) and endothelial cells as CD31+ (*) by immunofluorescence on adherent cells shown in (**c**) with anti-CD31 (red) and anti-CD45 (green) antibodies. (**e**) Quantification of SVF immunophenotyping (**d**) showing reduced frequency of ASCs among viable WAT cells. (**f**) The i.p. WAT cells shown in (**c**) post confluence were induced to differentiate into white adipocytes (7 days) and stained with Oil red O. Note that white adipocytes (accumulating large lipid droplets) are rare upon treatment. Error bars: S.E.M. $^*P<0.05$ *versus* control. Scale bar: 50 μM

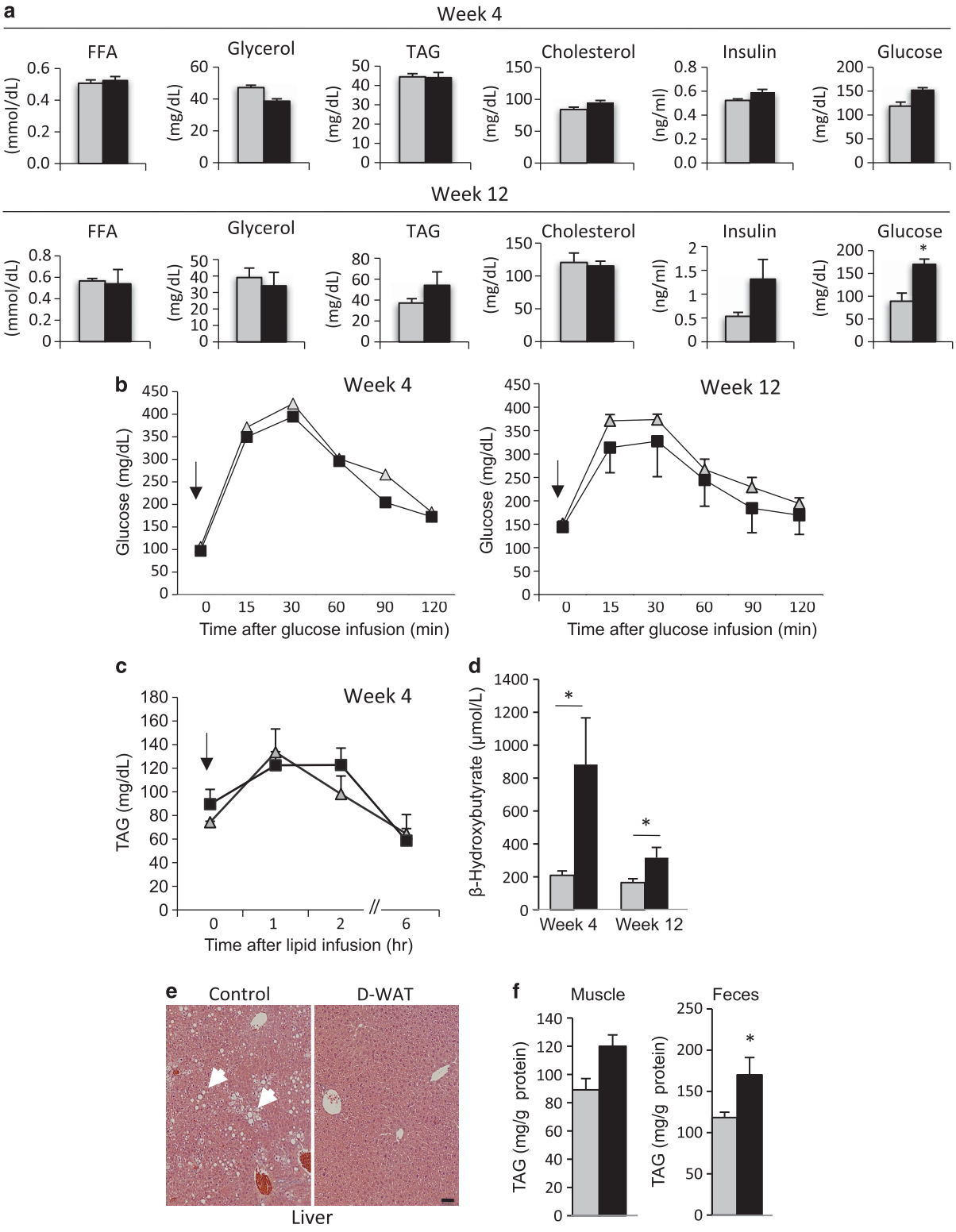

Figure 3 Lipid and glucose metabolism upon WAP depletion. D-WAT-treated (■) and control (□) mice analyzed at week 4 or week 12 as corresponding to Figure 2a timeline. (**a**) Steady-state levels of circulating free fatty acids (FFA), glycerol, triglycerides, cholesterol, insulin, and glucose in plasma. (**b**) Comparable kinetics of blood glucose clearance upon i.p. glucose infusion (arrow) into fasted mice. (**c**) Comparable kinetics of triglyceride clearance upon i.v. intralipid infusion (arrow) into fasted mice. (**d**) Circulating β-hydroxybutyrate increase in treated mice. (**e**) H&E-stained sections show reduced lipid (arrow) accumulation in the liver of treated mice. (**f**) Triacylglycerol (TAG) quantification in hind limb muscle and feces of control and treated mice. *$P<0.05$ *versus* control. Scale bar: 50 μm

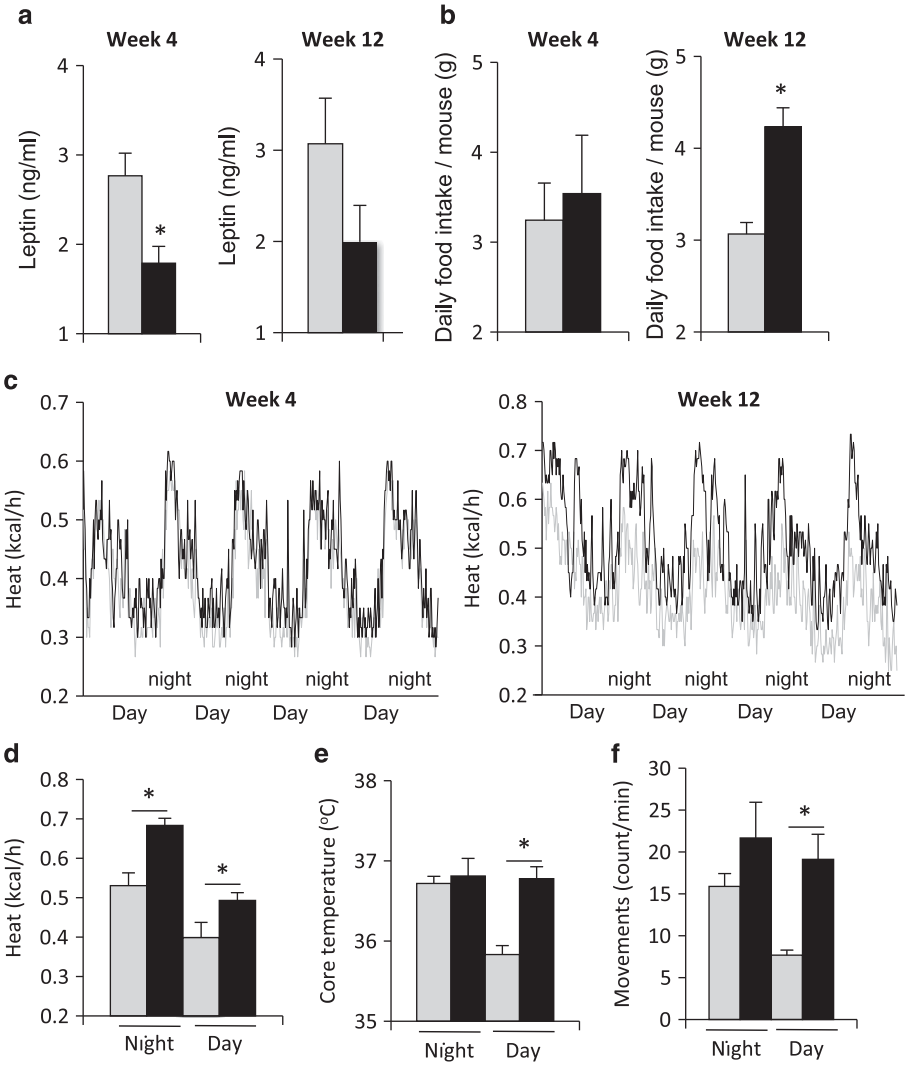

Figure 4 Energy intake and expenditure increase upon WAP depletion. D-WAT-treated (■) and control (▒) mice analyzed at week 4 or week 12 as corresponding to Figure 2a timeline. (**a**) Circulating leptin concentration decrease in treated mice. (**b**) Food consumption increase in treated mice analyzed over a 3-day period. (**c**) Heat expenditure increase in treated mice analyzed over a 4-day/night period (mean dark and light cycle values for 6 mice/group). (**d**) Data shown in (**c**) plotted as mean values averaged over the whole measurement period. (**e**) Core body temperature increase in treated mice (at week 4). Shown are mean values for representative 3-h intervals during dark and light cycles over a 72-h period. (**f**) Spontaneous locomotor activity increase in treated mice (at week 4). Plotted are mean values for representative 3-h intervals of dark and light cycles over a 72-h period. Error bars: S.E.M.; $*P<0.05$ *versus* control

A marked infiltration of s.c. WAT with brown-like adipocytes was observed in treated mice (Figure 5d). Consistent with this observation, the frequency of cells expressing UCP1 was found to be 12-fold higher in s.c. WAT of treated mice (Figures 5e and f). Frequency of UCP1 expression was also increased in i.p. WAT (Figure 5f). Quantitative real-time PCR indicated that Cidea, CD137, and PGC-1*α*, reported as markers of beige adipocytes,[43,44] were also induced in the WAT of treated animals (Figure 5g). These results indicate that, as a result of WAP depletion, WAT undergoes a partial conversion to beige fat that is particularly prominent in the s.c. depot.

WAP depletion spares beige adipocyte progenitors. Finally, we investigated the mechanism of adipocyte type switch upon WAP depletion. Recent studies indicate that beige adipocytes arise from a progenitor pool distinct from WAP rather than through adipocyte transdifferentiation.[11,45,46] It has been shown that beige adipocytes can be identified as CD137+UCP1+ cells with low expression of perilipin-1 (Plin1) among CD137−UCP1−Plin1+ white adipocytes.[8,32,33,43] To assess the content of beige adipocyte progenitors, we isolated SVF cells from s.c. WAT post D-WAT treatment, subjected them to brown adipogenesis induction in adherent culture, and then used immunofluorescence to measure UCP1 and Plin1 expression. As shown in Figure 6a, cells from control mice differentiated predominantly into UCP1-negative adipocytes with large lipid droplets coated with Plin1. In contrast, SVF from treated mice displayed predominant differentiation into UCP1+ adipocytes expressing low level of Plin1 (Figure 6a). Immunofluorescence revealed that the beige adipocyte marker CD137 is expressed in leukocytes present in the SVF of both treated and untreated mice. However, its

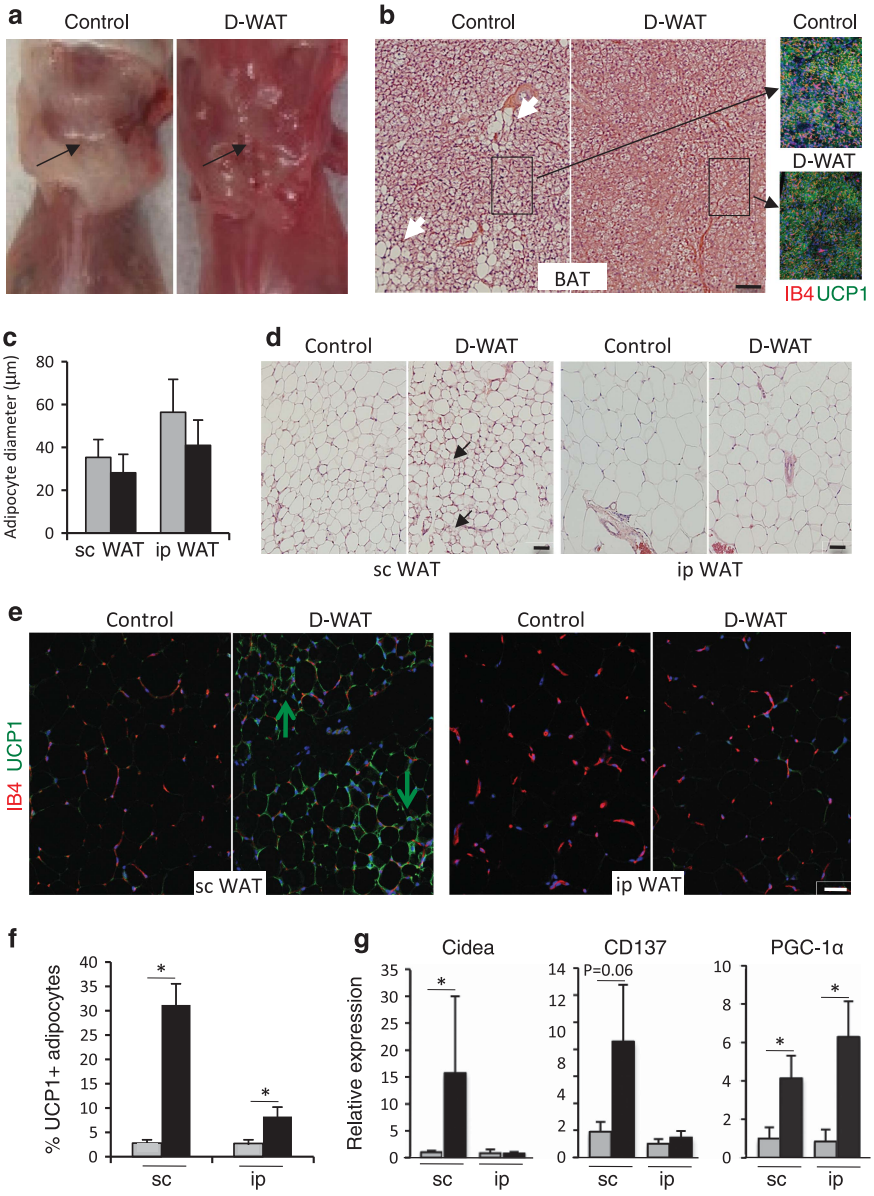

Figure 5 Adipose tissue browning upon WAP depletion. D-WAT-treated (■) and control (□) control mice analyzed at week 12 as corresponding to Figure 2a timeline. (**a**) Photographs of mouse upper backs (skin removed) revealing reduced lipid content in interscapular BAT (arrow) upon treatment. (**b**) H&E-stained paraffin BAT sections showing reduced size of lipid droplets (arrows) in brown adipocytes of treated mice. Inset: immunostaining shows comparable UCP1 expression (green) in control and treated mice. Isolectin B4 (red) stains endothelium. (**c**) Quantification of adipocyte size in WAT sections shows a trend for smaller s.c. and i.p. adipocyte size in treated mice. (**d**) H&E staining of WAT sections revealing areas containing brown-like adipocytes (arrows) in s.c. WAT of treated mice. (**e**) Immunofluorescence analysis of WAT sections with antibodies against UCP1 (green) and IB4 (red) confirming UCP1 expression in s.c. adipocytes (arrows) of treated mice. (**f**) Frequency of UCP1-expressing cells in s.c. WAT and i.p. WAT showing an increase in treated mice. (**g**) Quantitative PCR analysis of indicated gene expression normalized to 18S RNA showing induction in expression of beige adipocyte markers in s.c. and i.p. WAT of treated mice. Nuclei are blue. $^*P<0.05$ *versus* control. Scale bar: 50 μm

expression in adipocytes was induced selectively in the SVF derived from treated mice, but not from control mice (Figure 6b). These data indicate that progenitors of beige adipocytes are retained upon WAP depletion.

Recently, PDGFR*α*-positive stromal cells, not expressing PDGFR*β*, were identified in WAT as a distinct population of progenitors capable of differentiating into brown adipocytes.[22] To address the progenitor heterogeneity, we performed immunofluorescence analysis of WAT from untreated mice using two different PDGFR*α* antibodies. Consistent with published data,[22] our analysis shows that stromal cells expressing PDGFR*α*+ are distinct from PDGFR*β*+ WAP (Figure 6c). Whereas PDGFR*β*+ cells are predominantly localized in juxtaposition to the endothelium, PDGFR*α*+ cells are typically located in outer perivascular stroma layers often away from blood vessels (Figure 6d). By analyzing the SVF after D-WAT treatment, we observed a specific ablation of PDGFR*β*+ cells, whereas PDGFR*α*+ cells remained among adherent stromal cells (Figure 6e), indicating that WAT7 is specific for WAP.

It has been shown that beige adipocyte differentiation and activity in mouse s.c. WAT requires the PRDM16 transcription factor.[47] Using lentivirus expressing short hairpin RNA (shRNA), we silenced PRDM16 expression in s.c. ASCs and analyzed these cells in parallel with ASCs expressing untargeted shRNA (Figure 6f). Consistent with the lack of PRDM16 expression in WAP, its silencing did not significantly change cell sensitivity to D-WAT (Figure 6g). Confirming reported results,[47] PRDM16-silenced cells failed to differentiate into beige (UCP1+) adipocytes upon brown adipogenesis induction (Figure 6h). D-WAT treatment did not reduce the frequency of beige adipocyte differentiation in cells expressing untargeted shRNA, confirming that D-WAT spares beige adipocyte progenitors (Figure 6h). Upon D-WAT treatment, the frequency of PDGFRβ+ cells was reduced among PRDM16-silenced ASCs at least as much as among PRDM16-untargeted ASCs (Figure 6i). Combined, these data confirm that D-WAT specifically targets WAP. Interestingly, we detected an increase in the frequency of stromal PDGFRα+ cells in both s.c. and i.p. WAT of treated mice (Figure 6j). This suggests that not only the pool of PDGFRα+ stromal cells survives, but it also undergoes expansion upon PDGFRβ+ WAP depletion. We conclude that WAT browning in response to WAP depletion occurs because of recruitment of an alternative progenitor cell population, the PDGFRα+ PDGFRβ – stromal cells, which in s.c. WAT can differentiate into beige adipocytes.

Discussion

Previous studies have established a strategy to ablation of specific cell types based on 'hunter-killer' peptides.[28] Our group has successfully used cell-homing peptides coupled with a moiety $KLAKLAK_2$ that induces apoptosis.[30] Adipotide, a peptide that targets $_d$$KLAKLAK_2$ to WAT endothelium through the homing peptide CKGGRAKDC binding cell surface prohibitin, has been used for experimental obesity treatment.[26] Adipotide induces quick and substantial WAT mass regression and improves glucose tolerance that has been validated in mouse, rat, and several non-human primate models.[26,29,31,48] Here we use a novel hunter-killer peptide D-WAT, targeting WAP in both s.c. and i.p. WAT, to experimentally limit the pool of white adipocyte progenitors and determine whether the resulting white adipocyte shortage would have an effect on obesity development. By using D-WAT, we demonstrate that expansion of white adipocytes in a DIO model partly relies on WAP, suggesting that depletion of this progenitor population can be used as an approach to suppress WAT growth. It is important to contrast D-WAT with Adipotide that induces an acute reversal of experimental obesity that relapses upon treatment discontinuation.[26,31,48] Unlike Adipotide, D-WAT induces only a subtle WAT loss, whereas its suppression of WAT growth is long term, reflecting its impact on WAP, a distinct target cell population. Provided the endothelium-supporting function of perivascular ASCs,[5,19] the transient fat mass reduction observed during the treatment (Figure 2a) could be because of the temporary indirect effect of D-WAT on adipose vasculature.

WAT has remained controversial as a target in metabolic disease. Indeed, genetic models of lipodystrophy display dyslipidemia and the metabolic syndrome,[35,49,50] whereas thiazolidazines (TZD), promoting adipocyte differentiation, have antidiabetic activity.[51] The important distinction of our approach from models of total adipocyte deficiency is that it suppresses expansion of white adipocyte mass growth without causing lipodystrophy. Our data indicate that the adverse metabolic effects may be spared upon D-WAT treatment because of a skewed WAT development rather than its complete blockade. We demonstrate that WAP depletion results in WAT enrichment for thermogenic beige adipocytes. It has been shown that pharmacological treatments mildly reducing lipid content in white adipocytes, inducing WAT browning, and activating energy expenditure, improve metabolic function.[52] Recent findings indicating that TZD action partly relies on fat browning[53] is an illustration of the concept that a controlled modulation of adipocyte state can be not only safe but also beneficial.

No obvious adverse effects on mouse health have been detected upon D-WAT treatment. Increased appetite and the trend for lean mass increase (Figure 2b) rule out a possibility of caloric restriction being responsible for the WAT phenotype. This new approach to obesity suppression largely spares the adverse metabolic effects reported for genetic models of total adipose tissue deficiency.[35] In fact, treatment prevented dyslipidemia, partly because of fatty acid conversion to ketone bodies that can serve as an energy source for metabolically active tissues. Elevated basal glucose and insulin levels in nonstarved animals could be a reflection of the increased feeding. We conclude that WAT browning is unable to completely compensate for the changes in glucose homeostasis induced by WAP in the context of increased high-calorie diet intake. Because we observed changes not only in deep WAT depots, but also in intradermal WAT, it is possible that the resulting reduced thermo insulation and cold intolerance contributes to increased thermogenesis. The relative contribution of BAT, which undergoes browning in treated animals, to energy expenditure is also unclear. Because both BAT and beige adipocytes rely on SNS for their thermogenic activity, hypothalamic circuitry is likely to mediate the effects of WAP depletion. Future studies will help to better understand the complex physiology of the systemic response to WAP depletion.

Our study provides a fundamental insight into the function of adipocyte progenitor cells. It has been shown that brown-like adipocytes arise in s.c. WAT from progenitors *de novo* upon β-3 adrenergic stimulation.[11,45,46] A body of evidence indicates that developmentally distinct lineages of progenitor cells populate adipose depots with brown, beige, and white adipocytes.[22,54,55] Whereas WAPs expressing PDGFRβ (the population targeted by D-WAT) give rise to white adipocytes, PDGFRα was revealed as a marker of progenitors capable of differentiating into both white and brown-like adipocytes.[21,22] These precursor cells do not express PDGFRβ,[22] meaning that they are distinct from WAPs. Our results demonstrating mutually exclusive expression of PDGFRβ and PDGFRα on ASC subpopulations support this notion, and are consistent with the model according to which distinct adipocyte precursor cell populations predetermine the relative abundance of white and beige adipocytes. We show that although D-WAT treatment depletes WAP, it does not deplete the progenitors

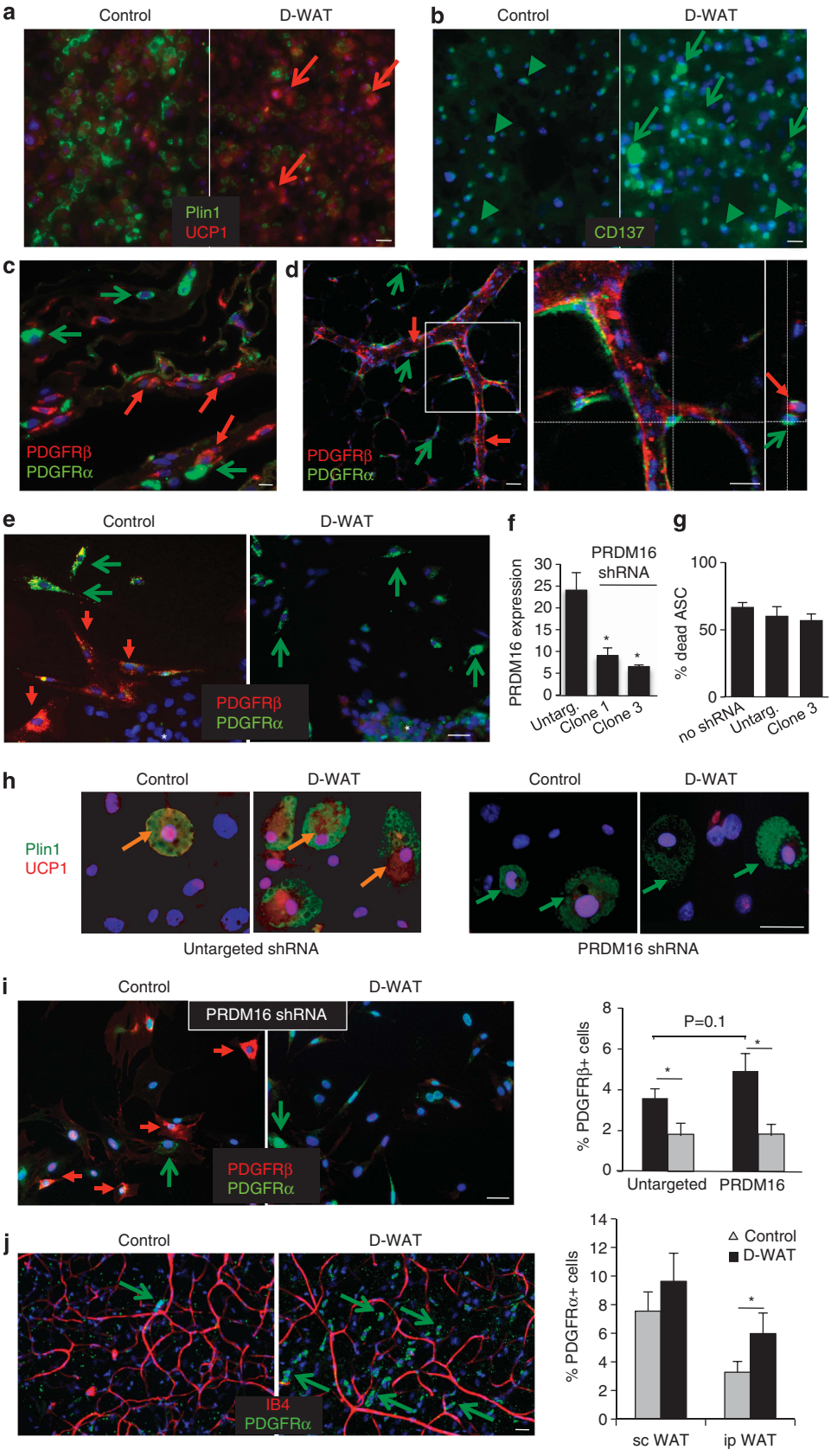
a
Control
D-WAT
Plin1
UCP1
b
Control
D-WAT
CD137
c
PDGFRβ
PDGFRα
d
PDGFRβ
PDGFRα
e
Control
D-WAT
PDGFRβ
PDGFRα
f
PRDM16 shRNA
PRDM16 expression
30
25
20
15
10
5
0
Untarg.
Clone 1
Clone 3
g
% dead ASC
100
50
0
no shRNA
Untarg.
Clone 3
h
Control
D-WAT
Plin1
UCP1
Untargeted shRNA
Control
D-WAT
PRDM16 shRNA
i
Control
D-WAT
PRDM16 shRNA
PDGFRβ
PDGFRα
% PDGFRβ+ cells
8
6
4
2
0
P=0.1
Untargeted
PRDM16
j
Control
D-WAT
IB4
PDGFRα
% PDGFRα+ cells
14
12
10
8
6
4
2
0
Control
D-WAT
sc WAT
ip WAT

of beige adipocytes. Based on the published observation that PDGFR*α*+ stromal cells are capable of differentiating into brown-like adipocytes *ex vivo*,[22] and on our observation that PDGFR*α*+ stromal cells are enriched in the WAT of treated animals, we conclude that PDGFR*α*+ ASCs serve as beige adipocyte progenitors. Interestingly, our data suggest that upon WAP depletion, PDGFR*α*+ ASCs undergo proliferation that may facilitate WAT population with beige adipocytes derived from these progenitors. Lineage tracing studies would be needed to confirm whether PDGFR*β*+PDGFR*α*− and PDGFR*α*−PDGFR*β*−. ASCs indeed represent distinct progenitor populations maintaining the pools of white and beige adipocytes, respectively.

A potential value of WAP depletion as an approach to obesity prevention, in particular in the context of aging and positive energy balance, remains to be further investigated. It should be noted that a similar physiological response could be achieved through approaches other than WAP depletion. Similar phenotypes have been previously demonstrated for adipose tissue browning achievable through WAT *β*-adrenergic signaling or through muscle and BAT stimulation.[38,56] Arguably, any controlled conversion of WAT into beige fat could be a viable strategy in treatment of obesity and the associated disorders.[6] Therefore, from a short-term clinical benefit point of view, pharmacological SNS stimulation[11,45,46] could be as effective. However, the conceptual distinction of obesity suppression via WAP depletion is that it changes the differentiation potential of WAT stroma. By enriching for beige adipocyte progenitors, WAP depletion predisposes WAT to undergo browning. Future studies will be needed to determine whether such WAT reprogramming is effective beyond the 3-month period analyzed in our study. This will determine whether inhibition of WAP with approaches based on the concept introduced here could complement conventional obesity therapies. As adipose progenitors functionally contribute to tumor microenvironment,[34] they could also be considered as a cancer therapy target.

Materials and Methods

Peptide synthesis and administration. Peptides were synthesized by conventional peptide chemistry, cyclized via cysteines, purified to >95% purity by HPLC and quality controlled (mass spectroscopy) by Celtek Peptides (Franklin, TN, USA). Cyclic CSWKYWFGEC was labeled using the EasyLink Cy3 Conjugation Kit (Abcam, Cambridge, MA, USA). Cyclic peptide $_d$CSWKYWFGEC-$_d$KLAKLAK$_2$ ($_d$WAT7-KLAKLAK$_2$) was designed based on previously described strategy,[26,30] but with all amino acids as D-enantiomers and with aminohexanoic acid NH-$(CH_2)_5$-CO as a linker (−). Peptide acetate salt powder was dissolved in phosphate-buffered saline (PBS) to 10 mM and aliquots were stored frozen until dilution in PBS, filtration, and use.

Animal studies. All animal studies were performed in accordance with the standards of the UTHealth Department of Comparative Medicine after review and approval of the protocol by Institutional Animal Care and Use Committee/Animal Welfare Committee. C57BL/6 male mice (6 weeks old) purchased from Jackson (Bar Harbor, ME, USA) have been fed 58 kcal% (fat) diet (Jackson D12331) for 3 months before the experiment. For the acute dose study (Figure 1), a single dose of D-WAT (2.4 mg) was administered s.c. and mouse tissues were analyzed the next day. For the efficacy experiment (Figures 2–6), 12 doses of D-WAT (1 mM) were administered s.c. into lower back (585 μg/injection/mouse) over a period of 4 weeks, after which animals were analyzed for a period of 8 more weeks. The efficacy experiment was performed three times with similar results. Body composition was measured by EchoMRI-100 T (Echo Medical Systems, Houston, TX, USA). Apo-Trace was administered according to the manufacturer's protocol (Sigma-Aldrich, St. Louis, MO, USA). Glucose tolerance test (6 mice/group) was performed as described,[26,37] with a glucometer (One Touch Ultra, Milpitas, CA, USA) upon injecting glucose (1 g/kg body weight) into overnight-fasted mice. Lipid tolerance test was performed as previously described[57] upon injecting 5.71 μl/g body weight of 20% intralipid (Sigma-Aldrich) into overnight-fasted mice. Indirect calorimetry (6 mice/group) studies were performed with OXYMAX (Columbus Instruments, Columbus, OH, USA) metabolic chambers as previously described.[26,37,58] Core body temperature and spontaneous locomotor activity was measured upon s.c. sensor implantation on the upper flank by using PDT-4000 G2 E-mitter sensors (MiniMitter, Resonics, Holliston, MA, USA).

Cell isolation, analysis, and culture. Tissues were resected and SVF were isolated from cell suspensions as previously described.[20,34] Mesenteric and epididymal WAT was used as i.p. WAT; inguinal WAT was used as s.c. WAT. Viable cells were cultured in DMEM/10% FBS on uncoated plastic overnight and, where indicated, treated with D-WAT and Apo-Trace. For flow cytometric analysis, cells were gated to exclude debris, cell clumps, and erythrocytes as previously described,[34] and then gated to identify apoptotic Apo-Trace+ cells according to the manufacturer's protocol (Sigma-Aldrich). For white adipogenesis induction, cells grown to confluence were cultured in medium containing 1.7 μM insulin, 0.5 mM IBMX, 1 μM dexamethasone, 0.2 μM indomethacin for 3 days and 1.7 μM insulin afterwards as previously described.[59] For brown adipogenesis induction, medium containing 5 μM dexamethasone, 850 nM insulin, 1 nM T3, and 1 μM rosiglitazone was used as previously described.[45] Oil red O staining was performed as previously described.[20]

Figure 6 Beige adipocyte progenitor retention upon WAP depletion. (**a** and **b**) Adherent s.c. SVF cells from D-WAT-treated and control mice analyzed at week 12 (as corresponding to Figure 2a timeline) were induced (4 days) to differentiate into brown adipocytes. (**a**) Anti-Plin1 (green)/anti-UCP1 (red) immunofluorescence shows preferential differentiation of ASCs from treated mice into beige (UCP1+) adipocytes (arrows), whereas mainly UCP1− adipocytes with large Plin1+ lipid droplets are observed for control mice. (**b**) Anti-CD137 immunofluorescence (green) reveals differentiation of ASCs from treated, but not from control, mice into beige adipocytes (arrows). Arrowheads indicate CD137+ leukocytes present in SVF from both control and treated mice. (**c**) Immunofluorescence analysis of s.c. WAT sections from a control mouse with ab51875 anti-PDGFRα (green) and anti-PDGFRβ (red) antibodies identifies PDGFRα+ and PDGFRβ+ stromal cells, as distinct populations. (**d**) Immunofluorescence analysis of whole mounts of i.p. WAT from a control mouse with AF1062 anti-PDGFRα (green) and anti-PDGFRβ (red) antibodies. Inset magnified on the right: confocal *Z*-stack projections of median series confirming that expression of PDGFRα and PDGFRβ on stromal cells is mutually exclusive. (**e**) Adherent s.c. SVF post D-WAT treatment were subjected to immunofluorescence analysis with anti-PDGFRα (green) and anti-PDGFRβ antibodies (red), demonstrating specific depletion of PDGFRβ+ cells. Endothelial colonies (*) are PDGFRα−PDGFRβ−. (**f**) Relative PRDM16 mRNA expression (normalized to 18S RNA) in s.c. SVF cells transduced with lentivirus expressing an untargeted shRNA (Untarg.) or shRNA clones 1 and 3 designed to silence PRDM16 expression measured by quantitative PCR. (**g**) The s.c. SVF cells not transduced (no shRNA) or transduced with untargeted shRNA or PRDM16 shRNA clone 3 were treated with D-WAT and cell death was quantified based on Trypan blue positivity. (**h**) Adherent s.c. SVF cells transduced with untargeted shRNA or PRDM16 shRNA (clone 3) were untreated (Control) or treated with D-WAT and then induced to differentiate into brown adipocytes (8 days), fixed, and subjected to anti-Plin1 (green)/anti-UCP1 (red) immunofluorescence. Note that UCP1 expression (orange arrows) is not observed in PRDM16 shRNA adipocytes (green arrows). (**i**) Adherent s.c. SVF cells transduced with untargeted shRNA or PRDM16 shRNA (clone 3) were untreated (Control) or treated with D-WAT and then subjected to immunofluorescence analysis with anti-PDGFRα (green) and anti-PDGFRβ antibodies (red). Images (left) demonstrate the retention of PDGFRβ+ cells (red arrows) upon PRDM16 silencing and their depletion upon D-WAT treatment; the graph (right) is data quantification. (**j**) Immunofluorescence analysis of s.c. WAT whole mounts with anti-PDGFRα antibody (green) and IB4 (red) reveals higher numbers of PDGFRα+ stromal cells (arrows) in treated mice. The graph (right) shows quantified frequencies of PDGFRα+ cells among nucleated cells of s.c. and i.p. WAT. Nuclei are blue. *$P<0.05$. Scale bar: 50 μm

Short hairpin RNA lentiviral vectors. PRMD16 silencing experiments were performed with lentiviral pLKO.1 vectors from the RNAi Consortium (TRC) lentiviral shRNA library (Open Biosystems, Lafayette, CO, USA). Oligonucleotide ID TRCN0000#58, referred to as PRMD16 C1; oligonucleotide ID TRCN0000#60, referred to as PRMD16 C3. GFP-shRNA PLKO.1 was used as untargeted shRNA control. Packaging vectors pCCLsin.PTT.PGK.EGFP.Wpre, pMDLg/pRRE, pRSV-Rev, and pMD2.VSVG (Addgene, Cambridge, MA, USA) were used for lentivirus production by transiently transfecting 293-Lentix cells (Xfect, Clontech, Mountain View, CA, USA) for 16 h, and harvesting viral particles 24 and 48 h later. Recombinant particles filtered through 0.45 μm pore cellulose acetate membranes and concentrated by ultracentrifugation for 2 h at 50 000 $\times g$ were used for transduction, drug selection, and reporter gene expression confirmation as previously described.

Tissue analysis. All steady-state plasma analyses were performed by Baylor Mouse Metabolism Core (Houston, TX, USA) under a fee-for-service contract. Food intake was measured as described previously.[26,37] Triglyceride quantification in muscle and feces was performed using a colorimetric kit from Biovision (Milpitas, CA, USA). Paraformaldehyde-fixed cells and formalin-fixed paraffin-embedded tissue sections were analyzed by immunofluorescence as previously described.[20,34] Whole mounts of WAT were prepared and analyzed as previously described.[24,60] Upon blocking, the following primary antibodies (4°C, 12 h) and secondary antibodies (RT, 1 h) diluted in PBS/0.05% Tween-20 were used: rat anti-CD44 from BD Pharmigen (San Jose, CA, USA; 1 : 100), rat anti-CD45 from eBioscience (San Diego, CA, USA; 1 : 100), goat anti-CD31 from Santa Cruz Biotechnology (Santa Cruz, CA, USA; 1 : 75), anti-Asp175-cleaved Caspase3 from Cell Signaling Technology (Beverly, MA, USA; 1 : 100); goat anti-DCN from R&D Systems (Minneapolis, MN, USA; 1 : 200); rabbit anti-UCP1 (Abcam, 1 : 1000); rabbit anti-Plin1 (Cell Signaling Technology, 1 : 100); rabbit anti-CD137 (Bioss, Woburn, MA, USA; 1 : 50); rat anti-PDGFRα ab51875 (Abcam, 1 : 100); goat anti-PDGFRα AF1062 (R&D Systems, 1 : 100), and rabbit anti-PDGFRβ ab32570 (Abcam, 1 : 100). Secondary antibodies used were: donkey Alexa488-IgG (Invitrogen, Grand Island, NY, USA; 1 : 150) and Cy3-IgG (Jackson ImmunoResearch, West Grove, PA, USA; 1 : 300). Biotinylated IB4 was from Vector Labs (Burlingame, CA, USA; 1 : 50) and used with Cy3-conjugated streptavidin as previously described.[24] Nuclei were stained with Hoechst 33258 or TO-PRO-3 (Invitrogen). Hematoxylin and eosin (H&E) staining was performed by histology CORE (IMM-UTH, Houston, TX, USA). Images were acquired with a confocal Leica TCS SP5 microscope/LAS AF software (Leica, Buffalo Grove, IL, USA) or Olympus IX70 inverted fluorescence microscope/MagnaFire software (Olympus, Center Valley, PA, USA). Fluorescence data were quantified with Amira 5.4 software (VSG) (Burlington, MA, USA). The mRNA from inguinal and epididymal WAT was isolated using TRIzol and converted to cDNA using SuperScript III Reverse Transcriptase (Invitrogen). Real-time qPCR analysis was performed based on TaqMan primers/Universal PCR Master Mix (Invitrogen) platform using ABI 7900 workstation and SDS 2.4 software (Applied BioSystems, Grand Island, NY, USA).

Statistical analysis. All tissue analyses included quantification of at least 10 microscopic fields of view and performed by two independent investigators. Graphpad Prism v.5.03 (La Jolla, CA, USA) and Microsoft Excel were used to graph data as mean $\pm$ S.D. or S.E.M. (as indicated) and to calculate *P*-values using homoscedastic Student's *t*-test. $P < 0.05$ was considered significant.

Conflict of Interest

MGK is a co-founder of Astrotide, Inc. developing D-WAT.

Acknowledgements. We thank W O'Brien and C Lee for technical help, as well as V Narkar, Q Tong, and R Berdeaux for insightful discussions. This work was supported by grants to MGK from American Heart Association (0835434N) and Cancer Prevention and Research Institute of Texas (RP100400), as well as to MMC Core at BCM under DRC (P30 DK079638).

1. Wisse BE, Kim F, Schwartz MW. Physiology. An integrative view of obesity. *Science* 2007; **318**: 928–929.
2. Friedman JM. Obesity: causes and control of excess body fat. *Nature* 2009; **459**: 340–342.
3. Sirin O, Kolonin MG. Treatment of obesity as a potential complementary approach to cancer therapy. *Drug Discov Today* 2013; **11**: 567–573.
4. Dolgin E. A history of drugs on the weight list. *Nat Med* 2012; **18**: 843.
5. Daquinag AC, Zhang Y, Kolonin MG. Vascular targeting of adipose tissue as an anti-obesity approach. *Trends Pharmacol Sci* 2011; **32**: 300–307.
6. Ducharme NA, Bickel PE. Lipid droplets in lipogenesis and lipolysis. *Endocrinology* 2008; **149**: 942–949.
7. Rosen ED, Spiegelman BM. What we talk about when we talk about fat. *Cell* 2014; **156**: 20–44.
8. Cinti S. Between brown and white: novel aspects of adipocyte differentiation. *Ann Med* 2011; **43**: 104–115.
9. Sun K, Kusminski CM, Scherer PE. Adipose tissue remodeling and obesity. *J Clin Invest* 2011; **121**: 2094–2101.
10. Spalding KL, Arner E, Westermark PO, Bernard S, Buchholz BA, Bergmann O *et al.* Dynamics of fat cell turnover in humans. *Nature* 2008; **453**: 783–787.
11. Wang QA, Tao C, Gupta RK, Scherer PE. Tracking adipogenesis during white adipose tissue development, expansion and regeneration. *Nat Med* 2013; **19**: 1338–1344.
12. Kras KM, Hausman DB, Hausman GJ, Martin RJ. Adipocyte development is dependent upon stem cell recruitment and proliferation of preadipocytes. *Obes Res* 1999; **7**: 491–447.
13. Gimble JM, Katz AJ, Bunnell BA. Adipose-derived stem cells for regenerative medicine. *Circ Res* 2007; **100**: 1249–1260.
14. Bianco P, Robey PG, Simmons PJ. Mesenchymal stem cells: revisiting history, concepts, and assays. *Cell Stem Cell* 2008; **2**: 313–319.
15. Caplan AI, Correa D. The MSC: an injury drugstore. *Cell Stem Cell* 2011; **9**: 11–15.
16. Kolonin MG, Simmons PJ. Combinatorial stem cell mobilization. *Nat Biotechnol* 2009; **27**: 252–253.
17. Rodeheffer MS, Birsoy K, Friedman JM. Identification of white adipocyte progenitor cells *in vivo*. *Cell* 2008; **135**: 240–249.
18. Tang W, Zeve D, Suh JM, Bosnakovski D, Kyba M, Hammer RE *et al.* White fat progenitor cells reside in the adipose vasculature. *Science* 2008; **322**: 583–586.
19. Traktuev D, Merfeld-Clauss S, Li J, Kolonin M, Arap W, Pasqualini R *et al.* A population of multipotent CD34-positive adipose stromal cells share pericyte and mesenchymal surface markers, reside in a periendothelial location, and stabilize endothelial networks. *Circ Res* 2008; **102**: 77–85.
20. Daquinag AC, Zhang Y, Amaya-Manzanares F, Simmons PJ, Kolonin MG. An isoform of decorin is a resistin receptor on the surface of adipose progenitor cells. *Cell Stem Cell* 2011; **9**: 74–86.
21. Berry R, Rodeheffer MS. Characterization of the adipocyte cellular lineage *in vivo*. *Nat Cell Biol* 2013; **15**: 302–308.
22. Lee YH, Petkova AP, Mottillo EP, Granneman JG. *In vivo* identification of bipotential adipocyte progenitors recruited by beta3-adrenoceptor activation and high-fat feeding. *Cell Metab* 2012; **15**: 480–491.
23. Kolonin MG, Sun J, Do KA, Vidal CI, Ji Y, Baggerly KA *et al.* Synchronous selection of homing peptides for multiple tissues by in vivo phage display. *FASEB J* 2006; **20**: 979–981.
24. Azhdarinia A, Daquinag AC, Tseng C, Ghosh S, Amaya-Manzanares F, Sevick-Muraca E *et al.* A peptide probe for targeted brown adipose tissue imaging. *Nat Comm* 2013; **4**: 2472–2482.
25. Staquicini FI, Cardo-Vila M, Kolonin MG, Trepel M, Edwards JK, Nunes DN *et al.* Vascular ligand-receptor mapping by direct combinatorial selection in cancer patients. *Proc Natl Acad Sci USA* 2011; **108**: 18637–18642.
26. Kolonin MG, Saha PK, Chan L, Pasqualini R, Arap W. Reversal of obesity by targeted ablation of adipose tissue. *Nat Med* 2004; **10**: 625–632.
27. Arap W, Kolonin MG, Trepel M, Lahdenranta J, Cardo-Vila M, Giordano RJ *et al.* Steps toward mapping the human vasculature by phage display. *Nat Med* 2002; **8**: 121–127.
28. Ellerby HM, Bredesen DE, Fujimura S, John V. Hunter-killer peptide (HKP) for targeted therapy. *J Med Chem* 2008; **51**: 5887–5892.
29. Barnhart KF, Christianson DR, Hanley PW, Driessen WH, Bernacky BJ, Baze WB *et al.* A peptidomimetic targeting white fat causes weight loss and improved insulin resistance in obese monkeys. *Sci Transl Med* 2011; **3**: 108–112.
30. Ellerby HM, Arap W, Ellerby LM, Kain R, Andrusiak R, Rio GD *et al.* Anti-cancer activity of targeted pro-apoptotic peptides. *Nat Med* 1999; **5**: 1032–1038.
31. Kim DH, Woods SC, Seeley RJ. Peptide designed to elicit apoptosis in adipose tissue endothelium reduces food intake and body weight. *Diabetes* 2010; **59**: 907–915.
32. Cannon B, Nedergaard J. Brown adipose tissue: function and physiological significance. *Physiol Rev* 2004; **84**: 277–359.
33. Gesta S, Tseng YH, Kahn CR. Developmental origin of fat: tracking obesity to its source. *Cell* 2007; **131**: 242–256.
34. Zhang Y, Daquinag AC, Amaya-Manzanares F, Sirin O, Tseng C, Kolonin MG. Stromal progenitor cells from endogenous adipose tissue contribute to pericytes and adipocytes that populate the tumor microenvironment. *Cancer Res* 2012; **72**: 5198–5208.
35. Asterholm IW, Halberg N, Scherer PE. Mouse models of lipodystrophy key reagents for the understanding of the metabolic syndrome. *Drug Discov Today* 2007; **4**: 17–24.
36. Friedman JM, Halaas JL. Leptin and the regulation of body weight in mammals. *Nature* 1998; **395**: 763–770.
37. Xu Y, O'Brien WG 3rd, Lee CC, Myers MG Jr, Tong Q. Role of GABA release from leptin receptor-expressing neurons in body weight regulation. *Endocrinology* 2012; **153**: 2223–2233.

38. Koncarevic A, Kajimura S, Cornwall-Brady M, Andreucci A, Pullen A, Sako D *et al.* A novel therapeutic approach to treating obesity through modulation of TGFbeta signaling. *Endocrinology* 2012; **153**: 3133–3146.
39. Cohen P, Levy JD, Zhang Y, Frontini A, Kolodin DP, Svensson KJ *et al.* Ablation of PRDM16 and beige adipose causes metabolic dysfunction and a subcutaneous to visceral fat switch. *Cell* 2014; **156**: 304–316.
40. Orci L, Cook WS, Ravazzola M, Wang MY, Park BH, Montesano R *et al.* Rapid transformation of white adipocytes into fat-oxidizing machines. *Proc Natl Acad Sci USA* 2004; **101**: 2058–2063.
41. Cinti S. Transdifferentiation properties of adipocytes in the adipose organ. *Am J Physiol Endocrinol Metab* 2009; **297**: 977–986.
42. Yoneshiro T, Aita S, Matsushita M, Kayahara T, Kameya T, Kawai Y *et al.* Recruited brown adipose tissue as an antiobesity agent in humans. *J Clin Invest* 2013; **123**: 3404–3408.
43. Wu J, Bostrom P, Sparks LM, Ye L, Choi JH, Giang AH *et al.* Beige adipocytes are a distinct type of thermogenic fat cell in mouse and human. *Cell* 2012; **150**: 366–376.
44. Fisher FM, Kleiner S, Douris N, Fox EC, Mepani RJ, Verdeguer F *et al.* FGF21 regulates PGC-1alpha and browning of white adipose tissues in adaptive thermogenesis. *Genes Dev* 2012; **26**: 271–281.
45. Kajimura S, Seale P, Kubota K, Lunsford E, Frangioni JV, Gygi SP *et al.* Initiation of myoblast to brown fat switch by a PRDM16-C/EBP-beta transcriptional complex. *Nature* 2009; **460**: 1154–1158.
46. Seale P, Bjork B, Yang W, Kajimura S, Chin S, Kuang S *et al.* PRDM16 controls a brown fat/skeletal muscle switch. *Nature* 2008; **454**: 961–967.
47. Seale P, Conroe HM, Estall J, Kajimura S, Frontini A, Ishibashi J *et al.* Prdm16 determines the thermogenic program of subcutaneous white adipose tissue in mice. *J Clin Invest* 2011; **121**: 96–105.
48. Kim DH, Sartor MA, Bain JR, Sandoval D, Stevens RD, Medvedovic M *et al.* Rapid and weight-independent improvement of glucose tolerance induced by a peptide designed to elicit apoptosis in adipose tissue endothelium. *Diabetes* 2012; **61**: 2299–2310.
49. Pajvani UB, Trujillo ME, Combs TP, Iyengar P, Jelicks L, Roth KA *et al.* Fat apoptosis through targeted activation of caspase 8: a new mouse model of inducible and reversible lipoatrophy. *Nat Med* 2005; **11**: 797–803.
50. Moitra J, Mason MM, Olive M, Krylov D, Gavrilova O, Marcus-Samuels B *et al.* Life without white fat: a transgenic mouse. *Genes Dev* 1998; **12**: 3168–3181.
51. Tontonoz P, Spiegelman BM. Fat and beyond: the diverse biology of PPARgamma. *Annu Rev Biochem* 2008; **77**: 289–312.
52. Reilly SM, Chiang SH, Decker SJ, Chang L, Uhm M, Larsen MJ *et al.* An inhibitor of the protein kinases TBK1 and IKK-varepsilon improves obesity-related metabolic dysfunctions in mice. *Nat Med* 2013; **19**: 313–321.
53. Qiang L, Wang L, Kon N, Zhao W, Lee S, Zhang Y *et al.* Brown remodeling of white adipose tissue by SirT1-dependent deacetylation of Ppargamma. *Cell* 2012; **150**: 620–632.
54. Sanchez-Gurmaches J, Hung CM, Sparks CA, Tang Y, Li H, Guertin DA. PTEN loss in the Myf5 lineage redistributes body fat and reveals subsets of white adipocytes that arise from Myf5 precursors. *Cell Metab* 2012; **16**: 348–362.
55. Shan T, Liang X, Bi P, Zhang P, Liu W, Kuang S. Distinct populations of adipogenic and myogenic Myf5-lineage progenitors in white adipose tissues. *J Lipid Res* 2013; **54**: 2214–2224.
56. Vegiopoulos A, Muller-Decker K, Strzoda D, Schmitt I, Chichelnitskiy E, Ostertag A *et al.* Cyclooxygenase-2 controls energy homeostasis in mice by de novo recruitment of brown adipocytes. *Science* 2010; **328**: 1158–1161.
57. Kotas ME, Jurczak MJ, Annicelli C, Gillum MP, Cline GW, Shulman GI *et al.* Role of caspase-1 in regulation of triglyceride metabolism. *Proc Natl Acad Sci USA* 2013; **110**: 4810–4815.
58. Tschop MH, Speakman JR, Arch JR, Auwerx J, Bruning JC, Chan L *et al.* A guide to analysis of mouse energy metabolism. *Nat Methods* 2012; **9**: 57–63.
59. Hemati N, Ross SE, Erickson RL, Groblewski GE, MacDougald OA. Signaling pathways through which insulin regulates CCAAT/enhancer binding protein alpha (C/EBPalpha) phosphorylation and gene expression in 3T3-L1 adipocytes. Correlation with GLUT4 gene expression. *J Biol Chem* 1997; **272**: 25913–25919.
60. Daquinag AC, Souza GR, Kolonin MG. Adipose tissue engineering in three-dimensional levitation tissue culture system based on magnetic nanoparticles. *Tissue Eng Part C Methods* 2013; **19**: 336–344.